# Mechanism and Kinetics of the Reactions of $NO_2$ or $HNO_3$ with Alumina as a Mineral Dust Model Compound

**Christoph Börensen,[†,‡] Ulf Kirchner,[†] Volker Scheer,[†] Rainer Vogt,[*,†] and Reinhard Zellner[‡]**

*Ford Forschungszentrum Aachen GmbH, Süsterfeldstr. 200, 52072 Aachen, Germany, Institut für Physikalische und Theoretische Chemie, Universität Essen, Universitätsstr. 5, 45177 Essen, Germany*

*Received: November 23, 1999; In Final Form: February 28, 2000*

The reaction of alumina as a model substance for mineral aerosols with $NO_2$ or $HNO_3$ was studied using diffuse reflectance infrared Fourier transform spectroscopy (DRIFTS). The formation of nitrate on the $Al_2O_3$ surface was observed in both cases. In addition, during the initial phase of the $NO_2$ reaction, intermediate nitrite formation was observed. The DRIFTS data provide insight into the reaction mechanism, which involves reaction of surface OH groups, the formation of a $\{AlOOH\cdots NO_2\}$ adduct, and the formation of acidic OH groups. The reaction order in $NO_2$ of $1.86 \pm 0.1$ was determined from a quantitative kinetic evaluation of a series of experiments with $NO_2$ concentrations in the range of $10^{13}$ to $10^{15}$ molecules $cm^{-3}$. The reactive uptake coefficient, $\gamma$, was determined from the infrared absorbance, which was calibrated by ion chromatography, and from the $Al_2O_3$ Brunauer−Emmett-Teller (BET) surface area. $\gamma$ depended linearly on the $NO_2$ concentration and varied from $\gamma = 7.3 \times 10^{-10}$ to $1.3 \times 10^{-8}$ for $[NO_2] = 2.5 \times 10^{13}$ to $8.5 \times 10^{14}$ molecules $cm^{-3}$. Estimations of the atmospheric impact showed that at these above conditions ($\gamma = 10^{-9}$) nitrate formation on mineral aerosol from the $NO_2$ reaction would be negligible.

## Introduction

Mineral aerosol represents one of the largest mass fractions of the global aerosol. It consists of windblown soil and is produced mainly in the arid areas of our planet, in particular in the great deserts. Its annual production rate is estimated to be about 200 to 5000 Tg.[1−3] The smaller size fraction ($<20$ $\mu$m) may be transported over long distances[4] of up to 5000 km.[1] Mineral aerosol has been considered a nonreactive, hydrophobic surface.[5] Nevertheless, its impact on the atmospheric radiation budget and on the concentration of cloud condensation nuclei (CCN) has been discussed. Recently, its possible role as a surface for heterogeneous reactions has been considered.[6,7] For example, in a recent modeling study Dentener et al.[8] calculated that more than 40% of the total atmospheric nitrate in large areas is associated with mineral aerosol. However, their results still suffer from large uncertainties in the heterogeneous reaction rates. Evidence from field measurements also exists for a correlation of the aerosol nitrate content and the aerosol mineral fraction.[9,10] A correlation between the nitrate mass size distribution and the mineral aerosol distribution has also been reported.[11]

Mineral aerosol has a complex chemical and mineralogical composition[12] in which aluminum in the chemical form of alumosilicates contributes ~8% by mass.[4] Alumina has been chosen as model substance, for the present investigation. It has a defined chemical composition, and, mainly because of its relevance as supporting material for catalysts, its surface features have been investigated by infrared spectroscopy[13,14] and ab initio calculations.[15] Also, the heterogeneous reactions of chlorofluorocarbons with alumina produced by solid-fuel rocket engines have been discussed with regard to stratospheric ozone depletion.[16]

In this work the reaction of alumina with nitrogen oxides has been studied using diffuse reflectance infrared Fourier transform spectroscopy (DRIFTS). This technique does not require a pretreatment of the sample and has the advantage that the formation of surface products becomes in situ visible.[17,18] It was possible to obtain the reaction order from a kinetic analysis, and it was also possible to determine the reactive uptake coefficient by calibrating the infrared absorbance with ion chromatographic analysis of reacted samples.

The huge, potentially reactive surface of mineral aerosols may be a significant sink for nitrogen oxides in the atmosphere and consequently could influence the global photooxidant budget. The aim of this work was to reveal some of the kinetics and mechanism of such heterogeneous reactions.

## Experimental Section

Vibrational spectra were recorded in the spectral range from 4000 to 600 $cm^{-1}$ with a Bruker Equinox 55 FTIR Spectrometer equipped with an mercury cadmium telluride (MCT) detector and DRIFTS optics (model DRA-2CO, Harrick Scientific Corp.). The vacuum chamber (model HVC-DR3, Harrick Scientific Corp.) was connected to a standard flow system (Figure 1). Spectra were recorded at a resolution of 4 $cm^{-1}$, and 100 scans were averaged for each spectrum resulting in a time resolution of 1 min. To improve the time resolution for experiments with high $NO_2$ concentrations during the initial phase, only 50 scans were averaged.

Alumina powder was freshly prepared immediately before each experiment by grinding 200 mg $Al_2O_3$ (>99.9% $\gamma$-$Al_2O_3$, −100 mesh, Aldrich) for 5 min in a vibration ball mill (Graseby Specac.) using an agate mortar. For all experiments 100 mg ground alumina was placed in the sample holder of the vacuum cell using a filling device which was constructed according to

* Corresponding author. E-mail: rvogt@ford.com.
† Ford Forschungszentrum Aachen GmbH.
‡ Universität Essen.

10.1021/jp994170d CCC: $19.00 
Published on Web 05/02/2000

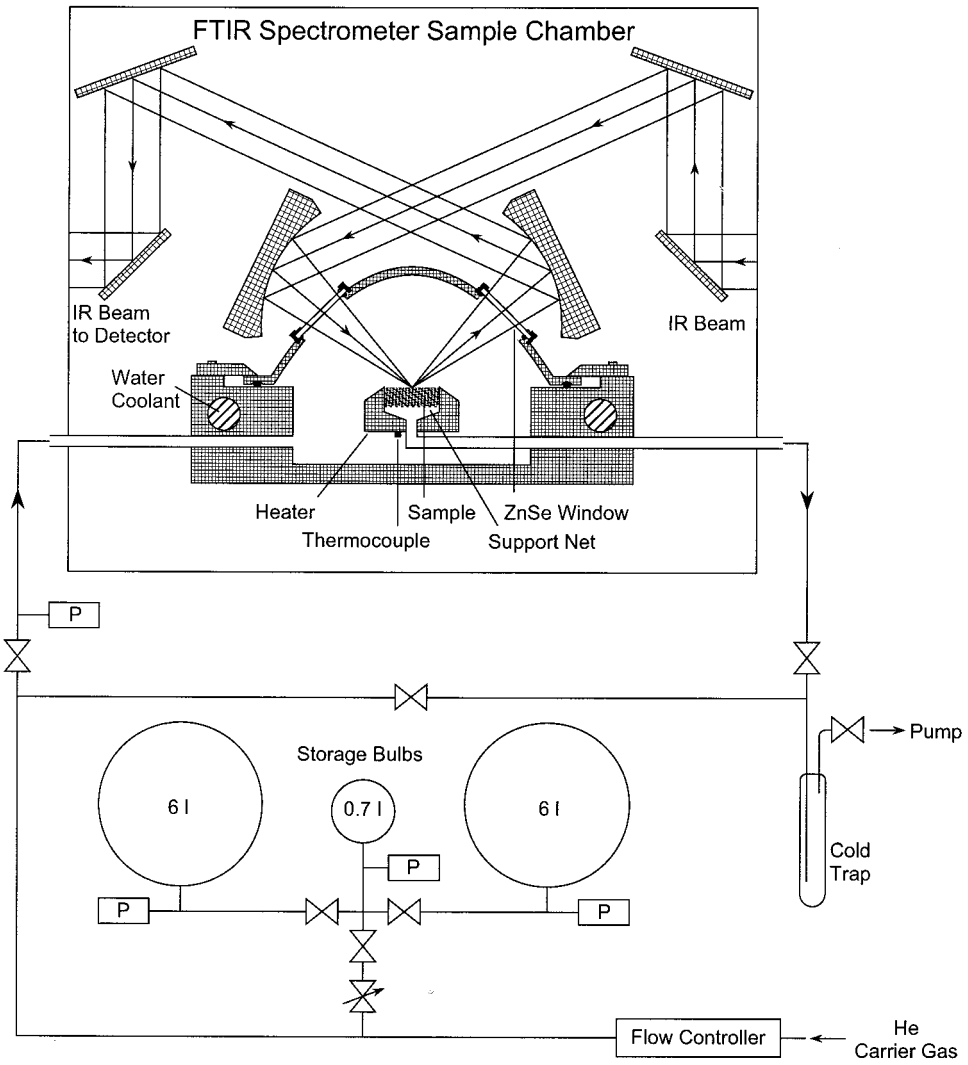


**Figure 1.** DRIFTS cell and flow system.

TeVrucht and Griffith[19] to obtain reproducible packing. The sample holder could be heated to 900 K, and the temperature was controlled by a thermocouple mounted directly underneath. A carrier gas stream of He (>99.999%, Messer-Griesheim) was passed through the sample powder at a flow rate of 1 standard cubic centimeter per minute (sccm) and a cell pressure of about 3.5 hPa. A mixture of $NO_2$ or $HNO_3$ with He was added to the carrier gas stream through a needle valve. The pressure drop in the calibrated storage bulb was measured, and the concentration of the reactive gases in the flow system was calculated. After the concentration had been adjusted, the valve to the large storage bulb was opened to maintain a constant leak rate during the experiment.

The specific surface area of ground alumina was determined according to the Brunauer−Emmett−Teller (BET) isotherm. The powder (800 mg) was degassed in a small glass tube of 4-mm diameter with an oil diffusion pump for 14 h at 413 K achieving a residual pressure of $2 \times 10^{-5}$ hPa. The system was protected from pump oil by a liquid nitrogen trap. The "dead space" over the powder was determined using nonadsorbing He. Ten points of the linear adsorption isotherm of nitrogen ($N_2$, >99.99% Messer-Griesheim) at 77 K were recorded in the $p/p^0$ range of 0.1 to 0.3 (MKS super Baratron pressure gauge). The specific surface area, $A_s$, was determined as $A_s = 10.0 \pm 0.8$ m$^2$ g using a molecular cross-sectional area of 0.162 nm$^2$ for nitrogen. Therefore, a typical sample had an absolute surface area of $A = 1.0$ m$^2$.

The absolute number of nitrate as well as nitrite ions formed during the reaction was determined by ion chromatography. The reacted alumina powder was sonicated in 10 mL of bidistilled water for 1 h. The filtered solution was analyzed using a Dionex DX 120 system, which was equipped with a Dionex AS 14 analytical column and a conductivity detector (CD 20) with detection stabilizer combined with an UV-absorbance detector (AD 20). Results from both detectors were averaged.

Nitrogen dioxide, $NO_2$, was prepared by adding excess oxygen ($O_2$, >99.998%, Messer-Griesheim) to nitric oxide (NO, >99.5%, Messer-Griesheim). Before mixing, the gases were passed through a cold trap held at 77 K to remove impurities such as water. After 10 h the $NO_2$ was condensed using an ice/acetone slurry, and the excess oxygen was removed by pumping. After the $NO_2$ was warmed to room temperature, the procedure was repeated twice. A potential impurity of $HNO_3$ could not be detected by IR spectroscopy (i.e., concentration of impurities was <1%). In the storage bulbs mixtures of He and the reactive gases of 0.5−2% were prepared at least 6 h before the experiment to ensure proper mixing.

Gas-phase nitric acid, $HNO_3$, was obtained from a mixture of concentrated sulfuric acid ($H_2SO_4$, A. C. S., Aldrich) and

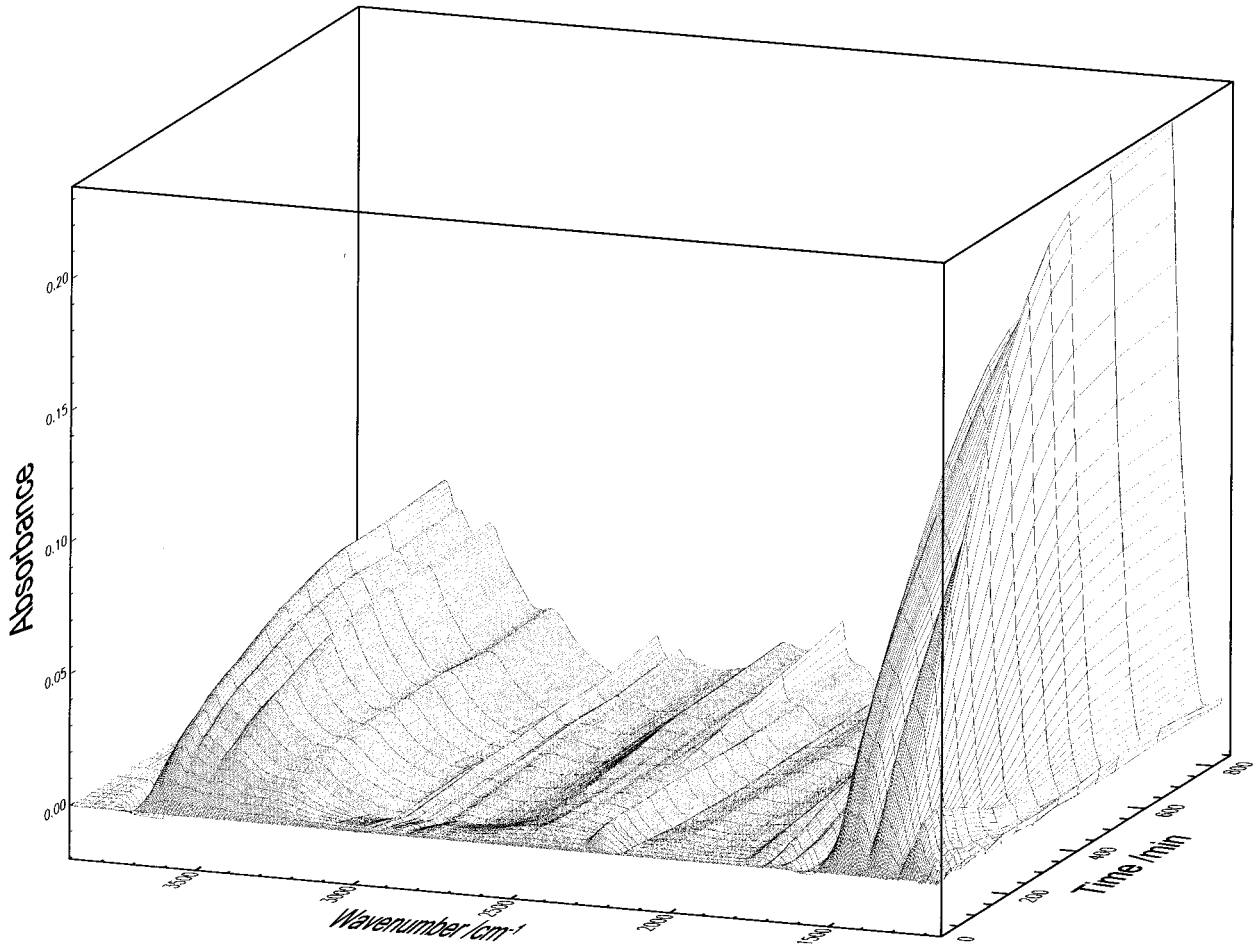


**Figure 2.** Absorption bands observed during the reaction of alumina with $NO_2$ as a function of reaction time ($[NO_2] = 1.35 \times 10^{14}$ molecules $cm^{-3}$).

nitric acid (>90%, Aldrich). Deuteriumoxide ($D_2O$, >99.96 at. % D, Aldrich) was used as supplied.

## Results and Discussion

**1. The Reaction of $NO_2$ with $Al_2O_3$.** *i. Observed Products.* At the beginning of each experiment, the freshly ground alumina was heated in the vacuum cell to 573 K for 1 h while the helium carrier gas was being passed through the sample. This procedure partially removes surface-adsorbed substances, in particular water, although a significant amount of water remains on the surface.[20] Reproducible surface conditions were achieved by this treatment. After the system was allowed to cool to room temperature the background spectrum of the unreacted alumina was recorded. With no reactive gases added to the system the baseline was constant for up to 2 days. After 5 h three weak absorption bands appeared in the range from 3000 to 2800 $cm^{-1}$, which could be attributed to the C−H stretch vibration of an organic impurity of unknown origin.

When $NO_2$ was added to the flow system several absorption bands were observed (Figures 2 and 3). The most prominent bands can be assigned to the vibration of the nitrate ion. The planar nitrate ion belongs to the point group $D_{3h}$ and has four fundamental vibrations: $\nu_1$ (symmetric stretch), $\nu_2$ (out-of-plane bend), $\nu_3$ (asymmetric stretch), and $\nu_4$ (in-plane bend), the last three of which are infrared active. The exact frequencies depend on the crystal structure and the associated cation.[21] For example, in $NaNO_3$ the typical frequencies $\nu_2$, 831 $cm^{-1}$, $\nu_3$, 1405 $cm^{-1}$, and $\nu_4$, 692 $cm^{-1}$ are observed. In Figures 2 and 3 the two most prominent bands in the region from 1550 to 1300 $cm^{-1}$ can be assigned to a split of the double degenerated asymmetric stretch vibration. This splitting has often been observed for the $\nu_3$ vibration and there are two explanations in the literature: 1) in the reaction of $NO_2$ with NaCl Vogt and Finlayson-Pitts[22] observed different kinetics for the two bands and concluded that they were due to two sites with a different lattice environment, and 2) the split can also be interpreted because of the loss of degeneration.[21,23,24] The reduction of the nitrate ion symmetry from $D_{3h}$ to $C_{2v}$ because of surface interaction causes the degenerated $\nu_3$ mode to split into four modes, of which two are IR active.[25] As explained in more detail below the results of this work show that the two bands grow at the same rate. Therefore, this is the most likely explanation for the observed spectra, in agreement with Goodman et al.[26] and Peters and Ewing.[25] Heating of the reacted sample to 773 K for 1 h at a cell pressure of 3 hPa and with a He carrier gas stream of 1 sccm directed through the alumina did not change the intensity of the absorption bands. This demonstrates that the nitrate is strongly bound to the surface. It has also been reported that treatment of the reacted alumina with oxygen at 150 °C did not alter the spectra observed initially.[27] The $\nu_1$ symmetric stretch vibration is infrared inactive but has nevertheless been observed in surface-bound nitrates.[22] In our experiments it is observed at 1050 $cm^{-1}$; however, because of the strong alumina lattice vibrations in the region from 1150 to 950 $cm^{-1}$, the IR sensitivity is very poor. We did not observe the weak $\nu_4$ in-plane bend vibration. The $\nu_2$ out-of-plane bend vibration, which

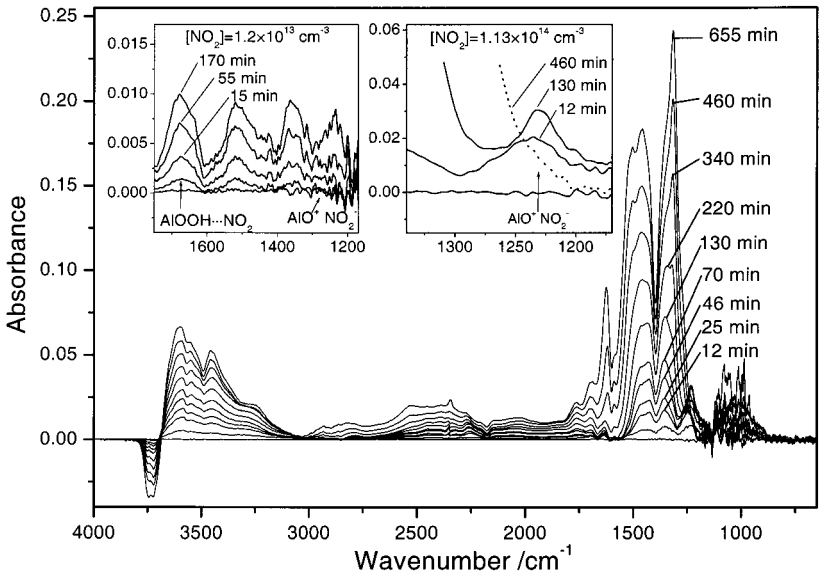


**Figure 3.** Absorption spectra recorded during the reaction of alumina with $NO_2$ ($[NO_2] = 1.13 \times 10^{14}$ molecules $cm^{-3}$) after a reaction time of 2, 12, 25, 46, 70, 130, 220, 340, 460 and 655 min. The right insert shows the decrease of the band initially observed band at 1235 $cm^{-1}$. The left insert shows the absorption band caused by $NO_2$ adsorbed on surface OH groups during an experiment with $[NO_2] = 1.2 \times 10^{13}$ molecules $cm^{-3}$.

is usually observed at 850 $cm^{-1}$ in the free nitrate ion, might be assigned to the weak shoulder located at 920 $cm^{-1}$. The frequency shift could be explained by the strong bonding of the surface-coordinated nitrate.

Another strong absorption band is observed at 1235 $cm^{-1}$. This band can be assigned to the asymmetric stretch vibration of the nitrite ion,[24] although its frequency differs from that of the free nitrite ion (1286 $cm^{-1}$). Similar frequency shifts have been reported depending on the metal ion coordination.[28] The nitrite ion belongs to the point group $C_{2v}$ and has three fundamental vibrations: $\nu_1$ (symmetric stretch), $\nu_2$ (bend), and $\nu_3$ (asymmetric stretch), the last two of which are infrared active. Typical frequencies[21] are $\nu_1$, 1327 $cm^{-1}$; $\nu_2$, 806 $cm^{-1}$; and $\nu_3$, 1286 $cm^{-1}$.

To further analyze the region from 1600 to 1150 $cm^{-1}$ ($\nu_3$ nitrate and $\nu_3$ nitrite bands) a curve-fitting procedure[29,30] using Lorenz and Gaussian curves was used to deconvolute overlapping bands. Every single spectrum of an experiment was fit by the Bruker "Opus" software using a Levenberg−Marquardt algorithm. An example of the fits is plotted in Figure 4a. The integrals of the recorded peaks are plotted in Figure 4b as a function of reaction time. As seen from this figure both of the broad $\nu_3$ nitrate bands grow at the same rate. Furthermore, it is possible to deconvolute the part of the $\nu_3$ band located at 1400−1250 $cm^{-1}$ into two main bands, which show a different kinetic behavior. The peak at 1354 $cm^{-1}$ is predominant in the beginning of the reaction, whereas at a later stage the 1313 $cm^{-1}$ peak grows faster, leading to an even larger integrated absorbance at the end of the reaction. This effect might be caused by differences in the lattice environments and surface sites with different reactivities.

The nitrite band at 1235 $cm^{-1}$ shows a completely different behavior. It grows fast in the beginning of the reaction, reaches a maximum, and decreases in intensity as the reaction proceeds. At the time when the nitrate absorption (1600−1250 $cm^{-1}$) is nearly saturated, the nitrite band is no longer noticeable. The reaction time after which the nitrite band has reached its maximum integrated absorbance strongly depends on the $NO_2$ concentration; at the highest concentrations used in this work, the maximum was reached after a few minutes, whereas at the lowest concentrations it did not even reach its maximum after 2 days. The occurrence of this band has also been reported and assigned to a nitrite species by Goodman et al.[26] and Miller and Grassian.[31] However, its subsequent decay has not been observed before, possibly because of the shorter reaction time used in these experiments. Moreover, the interference of the strong nitrate $\nu_3$ band, which broadens in the course of the reaction, might have made the small band undiscovered.

A weak band at 1690 $cm^{-1}$ can be assigned to surface-adsorbed nitrogen dioxide molecules $\{AlOOH\}\cdots NO_2$.[21] This band can clearly be observed at an early stage of the reaction (see insert, Figure 3). At a later stage it becomes superimposed by the stronger band at 1625 $cm^{-1}$ which can be assigned to the symmetric stretch vibration of the bidentate nitrate ion.[33] The shoulder at 1765 $cm^{-1}$ can be assigned to a combination vibration ($\nu_1 + \nu_4$) of the nitrate ion whereas the combination band at 2343 $cm^{-1}$ ($\nu_1 + \nu_3$) can be observed only at higher surface nitrate concentrations.

All absorption features in the spectral region from 3700 to 1800 $cm^{-1}$ are superimposed by a slight decrease of the very broad absorption of surface-adsorbed water. This loss of water during the reaction is caused by the carrier gas stream, because there is no correlation between the amount of water lost and the amount of nitrate formed. The strong absorption bands with peaks at 3600, 3550, and 3450 $cm^{-1}$ can be assigned to the O−H vibration of hydrogen-bonded OH groups of acids, such as $HNO_3$ or HONO.[21,32] These bands also resist heating to 300 °C for 1 h.

Another interesting observation is the decrease in absorption of a peak at 3745 $cm^{-1}$ and a shoulder at 3722 $cm^{-1}$. These absorption bands have been described before[33,34] and are attributed to a loss of OH surface species. According to an IR spectroscopic study by Tsyganenko and Mardilovich[13] these frequencies correspond to the O−H stretching vibration of OH groups coordinated with two aluminum atoms in coordination states VI and VI, or VI and IV, respectively. This assignment also agrees with observations made by Knözinger and Ratnasamy.[14] In an ab initio study on the interaction of water with alumina cluster models, Wittbrodt et al.[15] concluded that the observed frequencies were possibly caused by a single-bonded OH group.

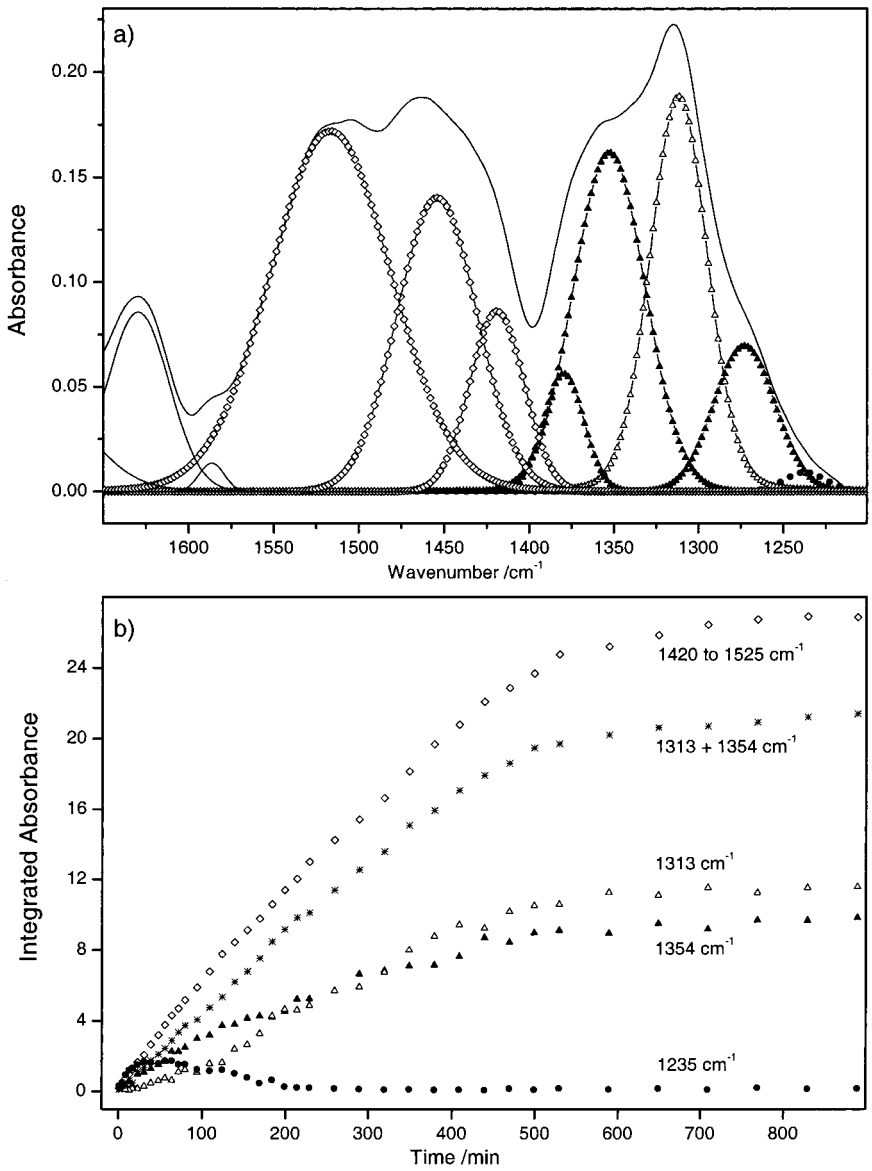


**Figure 4.** **a**, Absorption spectrum recorded in the reaction of $NO_2$ ($[NO_2] = 1.35 \times 10^{14}$ molecules $cm^{-3}$) with alumina after a reaction time of 1069 min. Lorenz and Gaussian functions were used to fit the split nitrate $\nu_3$ band. It was possible to separate the low-frequency nitrate band into two main parts and to reveal their different kinetic behavior (see Figure 4b). The symbols for the fitted curves correspond to their integrals plotted in Figure 4b. **b**, Integrated absorbance of bands recorded in the reaction of alumina with $NO_2$ ($[NO_2] = 1.35 \times 10^{14}$ molecules $cm^{-3}$) versus reaction time. The integration for each spectrum was performed using the curve-fit procedure as shown in panel a. The low-frequency band of the split nitrate absorption (1400−1250 $cm^{-1}$) can be separated in two parts with different kinetic behavior (triangles). The sum of these parts (stars), however, shows the same growth rate as the high-frequency nitrate band (1580−1400 $cm^{-1}$). The development of the intermediate nitrite band is shown by the circles.

The loss of surface OH groups (3745 and 3722 $cm^{-1}$) has been studied by isotopic substitution. An alumina sample has been treated with gaseous deuterium oxide ($D_2O$) for 3 h until no more changes in the IR spectrum were observed. The sample was exposed to $NO_2$ diluted by the carrier gas stream, after it was heated as described above for 1 h at 573 K. The spectra showed the formation of all main surface products, except that the OH absorption was shifted from 3745 to 2726 $cm^{-1}$ as would be expected for a loss of OD, which can be formed easily by a OH/OD exchange at the surface.[20,35,36] The temporal behavior of the surface OD groups was similar to that of the OH groups in the base study.

*ii. Mechanism.* A possible mechanism for the reaction of $NO_2$ on alumina includes the adsorption equilibrium of gas-phase $NO_2$ and physisorbed $NO_2$. The absorption band at 1690 $cm^{-1}$ observed at the early stage of the reaction (Figure 3) can be attributed to $NO_2$ which is attached to a surface OH group of the $\gamma$-alumina:

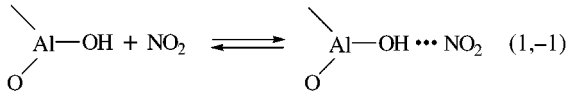


(1,–1)

In the next reaction step a disproportionation of two $NO_2$ molecules may result in surface-coordinated nitrate and nitrite species:

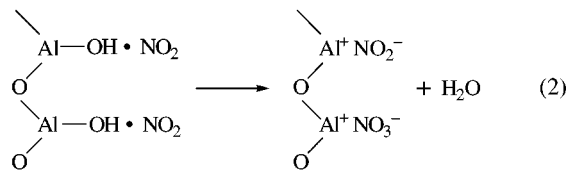


(2)

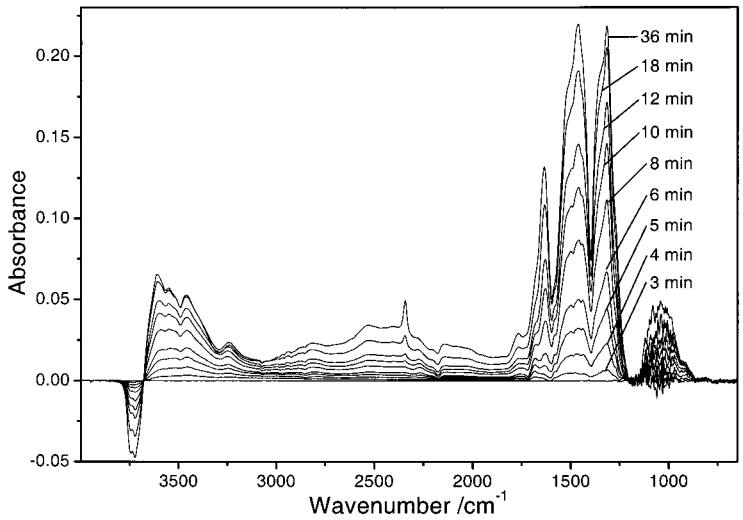


**Figure 5.** Absorption spectra recorded during the reaction of alumina with $HNO_3$ ($[HNO_3] = 8.2 \times 10^{13}$ molecules $cm^{-3}$) after a reaction time of 3, 4, 5, 6, 8, 10, 12, 18 and 36 min.

As suggested by Parkyns,[33] this disproportionation may also involve the formation of intermediate nitrosyl nitrate, $NO^+NO_3^-$, and can also be induced by the interaction with surface-adsorbed water. The nitrate and nitrite species are coordinated to the surface in various ways resulting in different absorption frequencies in the spectral range from 1200 to 1750 $cm^{-1}$. The observed acidic OH vibrations (3700−3300 $cm^{-1}$) are caused by adsorbed $HNO_3$ or HONO, which are in equilibrium (3, 4) with nitrate and nitrite ions and surface-adsorbed water:

$$\{(AlO)^+ NO_3^-\} + H_2O \rightleftharpoons \{AlOOH\cdots HNO_3\} \quad (3,-3)$$

$$\{(AlO)^+ NO_2^-\} + H_2O \rightleftharpoons \{AlOOH\cdots HONO\} \rightleftharpoons \{AlOOH\} + HONO \quad (4,-4)$$

The decrease of the initially observed nitrite peak (1235 $cm^{-1}$) can be explained by a change in pH at the surface caused by the loss of surface OH groups. During the course of the reaction the number density of {AlOOH} sites decreases and consequently equilibrium (4) is shifted to the right side with associated release of HONO to the gas phase. In contrast, the "sticky" nitric acid that is formed in equilibrium (3) remains at the surface. Further reactions of nitrous acid are also possible, that is, disproportionation to nitric acid and nitric oxide (NO).[37−39] In the current experimental setup no gas-phase analysis could be performed and therefore no conclusions on the gas-phase reaction products could be drawn.

*iii. Reaction Order.* The kinetics of the reaction of $NO_2$ with the alumina surface may be described by the general equation:

$$d\{NO_3^-\}/dt = k\{Al_2O_3\}^m [NO_2]^n \quad (5)$$

Concentrations marked with { } indicate surface species, whereas [ ] indicate the concentrations of gas-phase species, $k$ is the rate constant, and $m$ and $n$ are the reaction orders for alumina and nitrogen dioxide, respectively. Because the gas-phase concentration of the reactive gas is kept constant during the experiment and the number of nitrate ions formed is small relative to the number of reactive surface sites, $\{Al_2O_3\}$ (which is the case for the initial phase of the reaction), the latter can be assumed to be constant, and eq 5 easily integrates to:

$$\{NO_3^-\} = k\{Al_2O_3\}^m [NO_2]^n t \quad (6)$$

corresponding to a linear increase of $\{NO_3^-\}$ with time.

Because the infrared absorption cross-section is independent of $\{NO_3^-\}$, as confirmed in separate experiments, a plot of absorbance versus time should be linear. In Figure 6 the integrated absorbancies from 1570 to 1235 $cm^{-1}$ for four experiments with $NO_2$ concentrations in the range from $2 \times 10^{13}$ to $9 \times 10^{15}$ molecules $cm^{-3}$ are shown. In all cases the nitrate band grows at a constant rate during the initial phase of the reaction. Only at the end of the reaction does surface saturation occur. In experiments with low $NO_2$ concentrations a short initial period with a significantly higher reaction rate is observed (insert, Figure 6).

The reaction order may be determined from a bilogarithmic plot of the reaction rate versus the $NO_2$ concentration:

$$\log (d\{NO_3^-\}/dt) = \log k + m \log \{Al_2O_3\} + n \log [NO_2] \quad (7)$$

The reaction order $n$ for $NO_2$ on alumina was determined from the slope of Figure 7 to be $n = 1.86$ ($\pm 0.1$). If we consider that the assumption of a constant number density of reactive surface sites, $\{Al_2O_3\}$, results in a systematic lowering of the reaction rate and therefore an underestimation of the reaction order, within experimental uncertainties, the data can be interpreted as reflecting second-order kinetics. Second-order kinetics in $NO_2$ can be explained by the mechanism proposed in eq 2. In the first step surface-adsorbed $NO_2$ is formed, the concentraton of which is proportional to the $NO_2$ concentration in the gas phase. In the second reaction step a disproportionation of two $NO_2$ molecules occurs. This result is in sharp contrast to the value of 0.9 ($\pm 0.1$) determined by Goodman et al.[26] A possible reason for this discrepancy may be that Goodman et al. used a discontinuous experimental exposure in which $NO_2$ gas was inserted into a cell and replaced after an exposure time of 10 s. Their results for the reaction order of $NO_2$ depend on the assumption that the $NO_2$ pressure is approximately constant for that period and that sufficient unreacted alumina surface is available. An extrapolation of the reaction rates determined in our work to the higher concentrations used by Goodman et al. allows us to test whether this approach may be used. Although it can be shown that the assumption is valid for their lowest concentrations (i.e., at $[NO_2] = 7 \times 10^{14}$ molecules $cm^{-3}$ and $\gamma = 2.3 \times 10^{-8}$, 16% of the total $NO_2$ molecules contained in the cell volume have reacted within 10 s), this is not the case for the largest $NO_2$ concentration used in these experiments

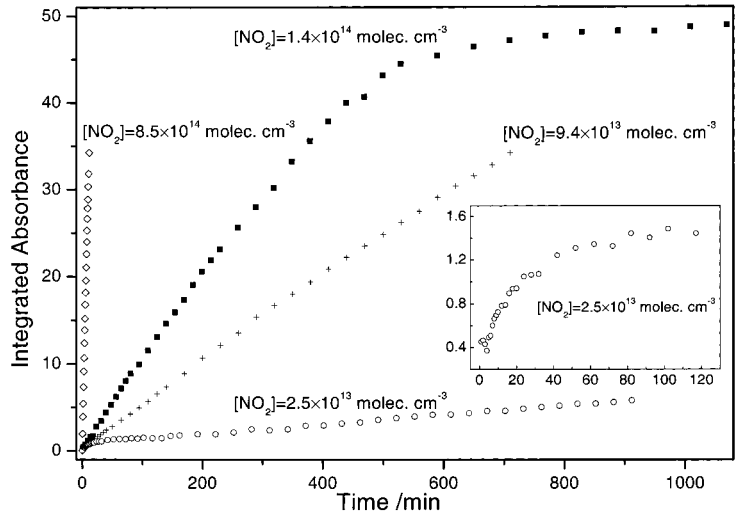


**Figure 6.** Integrated absorbance over the nitrate $\nu_3$ band (1550−1235 cm$^{-1}$) observed during the reaction of $NO_2$ with alumina. The results of four different experiments with $[NO_2] = 2.5 \times 10^{13}$, $9.4 \times 10^{13}$, $1.4 \times 10^{14}$, and $8.5 \times 10^{14}$ molecules cm$^{-3}$ are shown. In the insert the initial phase of a run with $[NO_2] = 2.5 \times 10^{13}$ molecules cm$^{-3}$ is displayed, indicating a higher initial reaction rate during the first 30 min.

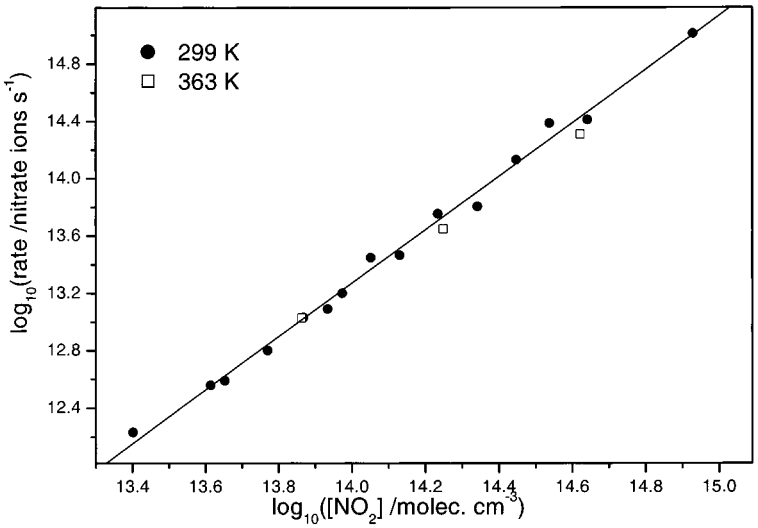


**Figure 7.** Bilogarithmic plot of the rate of nitrate formation as a function of $[NO_2]$. The rate of formation is given in ions s$^{-1}$ and has been calculated from the integrated absorbancies using a cross-section of of $f = 1.9$ ($\pm 0.2$) $\times 10^{16}$ (ions m$^{-2}$ integrated absorption units$^{-1}$). The reaction order in $NO_2$ was determined from a linear regression of this plot according to eq 11 and to be $n = 1.86 \pm 0.1$.

($[NO_2] = 1 \times 10^{16}$ molecules cm$^{-3}$, $\gamma = 3.0 \times 10^{-7}$). In this case more than 66% of the available $NO_2$ have reacted in 10 s, which leads to underestimation of the reaction rate in the experiments with larger $NO_2$ concentrations and therefore to underestimation of the reaction order.

The reaction order for the loss of OH was determined using the integrated band intensity from 3800 to 3690 cm$^{-1}$ in the same way as described above for the formation of nitrate. The reaction order in $NO_2$ determined from the loss of surface OH is $n_{OH} = 1.89$ ($\pm 0.1$), which is very close to second-order kinetics and in agreement with the proposed mechanism (eq 2).

Another possible explanation of second-order kinetics is that the $NO_2$ dimer, $N_2O_4$, which is in equilibrium with $NO_2$ in the gas phase, is the reactive species:

$$[N_2O_4] = K_{eq}\,[NO_2]^2 \qquad (8)$$

where $K_{eq} = 2.50 \times 10^{19}$ cm$^3$ molecule$^{-1}$ at 295 K.

$$N_2O_4 + 2\{(AlO)OH\} \rightarrow \{(AlO)^+\,NO_3^-\} + \{(AlO)^+\,NO_2^-\} + H_2O \qquad (9)$$

Analogous suggestions can be found in the literature for the reaction of $NO_2$ with NaCl.[22,41] To test whether this mechanism holds, three experiments were conducted at an elevated temperature (363 K), because the equilibrium constant strongly depends on the temperature and the fraction of $N_2O_4$, which is $1.2 \times 10^{-2}$ % at 299 K for $[NO_2] = 5 \times 10^{14}$ molecules cm$^{-3}$, drops to $2 \times 10^{-4}$ % at 363 K.[40] However, only a slight decrease of the reaction rates was observed under these conditions (Table 1 and Figure 7). Therefore, it can be concluded that gas-phase $N_2O_4$ is not the reactive species.

*iv. Uptake Coefficient.* To quantify the reaction rate $d\{NO_3^-\}/dt$ in terms of the reactive uptake coefficient the amount of nitrate on the sample was determined by ion chromatography. As already reported for the nitrate formation on NaCl, which also has been studied with DRIFTS,[22,41] a linear relationship was found between the integrated absorbance of the $\nu_3$ band (expressed in absorption units and not in integrated Kubelka−Munk units, which are usually used in DRIFT spectroscopy) and the $\{NO_3^-\}$ concentration:

$$(\text{integrated absorbance } \nu_3) \times f = \{NO_3^-\} \qquad (10)$$

**TABLE 1: Reactive Uptake Coefficients for the Reaction of $NO_2$ with $Al_2O_3$ at 299 K**

| | reaction rate | | | | |
|---|---|---|---|---|---|
| $[NO_2]$ ($10^{13}$ molec $cm^{-3}$) | $d[\nu_3$ Abs.$]/dt$[a] ($min^{-1}$) | $d\{NO_3^-\}/dt$[b] ($10^{12}$ ions $s^{-1}$) | $(dN(NO_2)/dt)$[c] ($10^{12}$ molec $s^{-1}$) | $Z$ $(NO_2)$[d] ($10^{21}$ molec $s^{-1}$) | $\gamma$ $(NO_2)$[e] ($10^{-9}$) |
| 1.21 | 0.0021 | 0.7 | 1.4 | 1.109 | 1.26 |
| 2.52 | 0.0053 | 1.7 | 3.4 | 2.311 | 1.47 |
| 4.12 | 0.0114 | 3.6 | 7.2 | 3.773 | 1.92 |
| 4.50 | 0.0123 | 3.9 | 7.8 | 4.124 | 1.89 |
| 5.90 | 0.0235 | 7.4 | 14.8 | 5.407 | 2.75 |
| 7.00 | 0.0333 | 10.6 | 21.2 | 6.415 | 3.29 |
| 7.30[f] | 0.0343 | 10.8 | 21.6 | 7.460 | 2.90[f] |
| 8.60 | 0.0427 | 13.6 | 27.2 | 7.881 | 3.44 |
| 9.43 | 0.0501 | 15.9 | 31.8 | 8.642 | 3.68 |
| 11.3 | 0.0886 | 28.1 | 56.2 | 10.33 | 5.45 |
| 13.5 | 0.1005 | 31.9 | 63.8 | 12.37 | 5.16 |
| 17.1 | 0.1795 | 57.0 | 114.0 | 15.71 | 7.26 |
| 17.7[f] | 0.1430 | 45.0 | 90.0 | 18.10 | 4.98[f] |
| 23.0 | 0.2436 | 77.3 | 154.6 | 21.08 | 7.34 |
| 28.0 | 0.4540 | 144.1 | 288.2 | 25.66 | 11.23 |
| 34.5 | 0.7679 | 243.8 | 487.6 | 31.60 | 15.43 |
| 41.8[f] | 0.6511 | 204.7 | 409.4 | 42.70 | 9.58[f] |
| 43.8 | 0.8136 | 258.3 | 516.6 | 40.09 | 12.84 |
| 84.9 | 3.2441 | 1030.0 | 2060.0 | 77.77 | 26.48 |

[a] Observed rate of nitrate formation (integrated absorbance units $min^{-1}$) obtained from the integrated absorbance (Abs.) of the nitrate $\nu_3$ vibrations. [b] Rate of nitrate formation from $\nu_3$ absorption calibrated by ion chromatography. [c] Rate of loss of gas-phase $NO_2$. [d] Collision rate for $NO_2$ with the surface. [e] Reactive uptake coefficient for $NO_2$ calculated according to eq 11. [f] Experiment performed at a higher temperature (363 K).

To calculate the factor $f$ for each experiment, the total number of nitrate ions on the sample after the reaction as determined by ion chromatography was divided by the integrated nitrate absorbance of the spectrum. The conversion factor $f$ was found to be independent of reaction time and $NO_2$ concentration as long as the experiment was completed at a stage for which the absorption of the nitrate band was still growing. A value of $f = 1.9\ (\pm 0.2) \times 10^{16}$ (ions $m^{-2}$ integrated absorption units$^{-1}$) was calculated. In two experiments $NO_2$ was added for 1 h after the nitrate band had already reached its maximum absorbance. In these runs additional nitrate formation was observed by ion chromatography, indicating that when the reaction is nearly completed some nitrate formation still occurs which is invisible to DRIFTS. This demonstrates that the IR beam interferes only with the top surface layers of the sample.[42] Therefore, the experiments were performed such that the whole sample that is analyzed by ion chromatography is exposed to the same concentration of reactive gases. In $NO_2$ at least 96% of the gas entering the cell passes through the sample without reaction. From ion chromatography analysis and the specific BET surface area of the alumina ($A_s = 10.0\ m^2\ g^{-1}$) it was found that a saturated sample contains a surface nitrate concentration of $2.3 \times 10^{18}$ ions $m^{-2}$. This concentration is in reasonable agreement with the results of Underwood et al.[39] [$(1.5-2) \times 10^{18}$ ions $m^{-2}$] and the value of $1.3 \times 10^{18}$ ions $m^{-2}$, which can be calculated from the results of Judeikis et al.[43] Assuming that one nitrate ion covers an area of $1.3 \times 10^{-19}\ m^2$ it can be calculated that about 30% of the alumina surface area is covered with nitrate at the end of the reaction.

A parameter often used in atmospheric chemistry to describe the overall kinetics of a heterogeneous reaction is the reaction probability, or reactive uptake coefficient, $\gamma$. This coefficient is defined as the number of reactive collisions with the surface ($dN(NO_2)/dt$) divided by the total number of surface collisions $Z$.

$$\gamma = (dN(NO_2)/dt)/Z \qquad (11)$$

The number of reactive collisions can be derived from the reaction rate for the formation of nitrate. With respect to the observed second-order kinetics and the proposed mechanism we assume that the rate of $NO_2$ loss in the gas phase is twice as high as the rate of nitrate formation. The total number of collisions can be calculated according to the kinetic gas theory:

$$Z = (1/4)\, A\, [G]\, ((8RT)/(\pi M_G))^{0.5} \qquad (12)$$

where $A$ is the sample surface, $[G]$ is the concentration of gas-phase species, and $M_G$ the molecular mass of the gas-phase reactant.

The uptake coefficient of the unreacted surface is expected to be independent of the reactant concentration only under the assumption of first-order kinetics. In the concentration range of this study ($[NO_2] = 1 \times 10^{13}$ to $8.5 \times 10^{14}$ molecules $cm^{-3}$) the reactive uptake $\gamma$ varies from $1.3 \times 10^{-9}$ to $2.6 \times 10^{-8}$ (Table 1 and Figure 8). These results are in the same order of magnitude as the ones recently reported by Underwood et al.,[39] but Underwood et al. did not observe the dependence of the uptake coefficient from $NO_2$ concentration. This may be explained because they determined only two uptake coefficients in the concentration range covered in this study.

In the derivation of the uptake coefficient we use the sample BET surface area, which is in close approximation to the reactive surface under atmospheric conditions. Judeikis et al.[43] determined the gas-wall collision efficiency for the reaction of alumina with $NO_2$ in a flow reactor from which a higher collision efficiency ($>1 \times 10^{-4}$) was calculated using the geometric proportions of the reactor. The gas-wall collision efficiency of Judeikis et al.[43] is therefore not suitable for calculations of the reaction rate of real atmospheric aerosol and cannot be compared with the results from the present study.

As described above, we also observed a short initial period with a higher reaction rate in experiments with lower $NO_2$ concentrations. We did not quantify this initial uptake because the amount of $NO_2$ converted during this period too small to have atmospheric relevance.

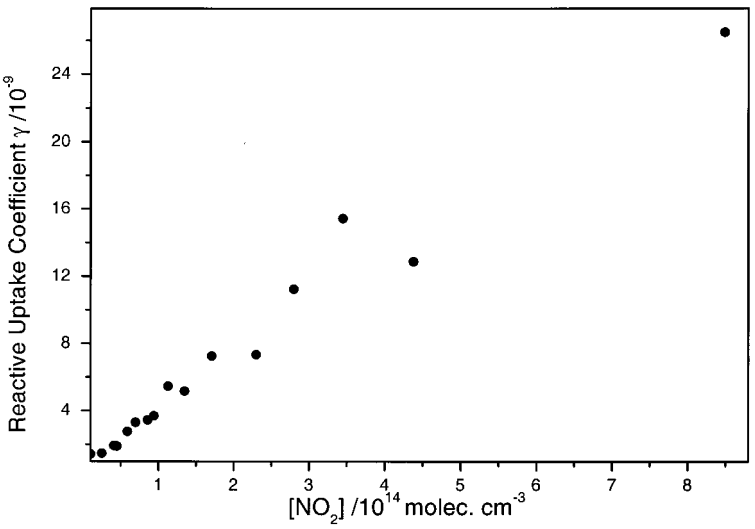


**Figure 8.** Reactive uptake coefficient for the reaction of alumina with $NO_2$ as a function of $[NO_2]$.

**2. The Reaction of $HNO_3$ with $Al_2O_3$.** Alumina samples used to study the reaction with $HNO_3$ were pretreated in the same manner as described above for the reaction with $NO_2$. The resulting spectra (Figure 5) showed the same main features: intense absorption bands of the split nitrate $\nu_3$ vibration in the range from 1570 to 1250 $cm^{-1}$, the nitrate $\nu_1 + \nu_3$ combination band at 2343 $cm^{-1}$, the loss of OH surface species at 3745 and 3722 $cm^{-1}$, and the increase of absorption caused by acidic OH groups. The nitrite peak at 1235 $cm^{-1}$ was not observed.

These observations can be interpreted by the reaction of $HNO_3$ with surface OH species (equilibrium reaction −3,3):

$$\{AlOOH\cdots HNO_3\} \rightleftharpoons \{(AlO)^+NO_3^-\} + H_2O \qquad (-3,3)$$

These experiments cannot distinguish whether $HNO_3$ reacts directly from the gas phase, or after physisorption and solution in surface-adsorbed water. However, Davies and Cox[44] recently showed that the reaction of $HNO_3$ with NaCl involves the ionic dissolution in the presence of surface-adsorbed water. From the current experiments it is evident that the $HNO_3$ reaction is much faster than that of $NO_2$; however, a determination of the reaction order and uptake coefficient was not possible because of limitations of the current experimental setup, which was constructed for quantitative analysis of slow reactions only.

## Conclusions and Atmospheric Implications

It was possible to observe in situ formation of nitrate, water, and intermediate nitrite in the reaction of $NO_2$ and $HNO_3$ with the alumina surface by using DRIFTS. The $NO_2$ and $HNO_3$ reactions are completed when the amount of nitrate formed is sufficient to cover ca. 30% of the surface, indicating that the reactions are limited to the surface layer. The reaction order in $NO_2$ was determined to be $n = 1.86$ ($\pm 0.1$), which within experimental error is interpreted to reflect second-order kinetics. This finding indicates a complex reaction mechanism involving intermediate surface products. The reactive uptake coefficient for the reaction of alumina with $NO_2$ was determined to be $\gamma = 1.3 \times 10^{-9}$ ... $\gamma = 2.6 \times 10^{-8}$ at $[NO_2] = 1.2 \times 10^{13}$ ... $8.5 \times 10^{14}$ molecules $cm^{-3}$, respectively. The relevance of the reaction of $NO_2$ with mineral aerosol in the atmosphere can be estimated with use of this uptake coefficient. Assuming a mineral dust concentration of 25 $\mu g\ m^{-3}$ and an average aerosol diameter of 3 $\mu m$ a nitrate mass of 0.0013 $\mu g\ m^{-3}$ would be formed within 2 weeks of atmospheric residence time. Under the conditions above ($\gamma = 10^{-9}$) nitrate formation on mineral aerosol from the $NO_2$ reaction would be negligible.

**Acknowledgment.** We are grateful to the Bundesministerium für Bildung und Forschung for partially funding this work with grant 07AF210A. We thank the Zentrallabor of the Ford Werke AG, Cologne, for conducting the ion chromatographic analysis.

## References and Notes

(1) Jonas, P. R.; Rohde, H. *Climate Change 1994*; Houghton, J. T., Ed.; Cambridge University Press: New York, 1995; Chapter Aerosol.
(2) d'Almeida, G. A. *J. Geophys. Res.* **1987**, *92*, 3017.
(3) Tegen, I.; Fung, I. *J. Geophys. Res.* **1994**, *D11*, 22, 897.
(4) Gomes, L.; Gilette, D. A. *Atmos. Environ.* **1993**, *16*, 2539.
(5) Bergametti, G.; Dulac, F. *IGACtivities* **1998**, *1*, 13.
(6) Zhang, Y.; Sunwoo, Y.; Kotamarthi, V.; Carmichael, G. R. *J. Appl. Meteorol.* **1994**, *33*, 813.
(7) Mamane, Y.; Gottlieb, J. *Atmos. Environ.* **1992**, *26A (9)*, 1763.
(8) Dentener, F. J.; Carmichael, G. R.; Zhang, Y.; Lelieveld, J. Crutzen, P. J. *J. Geophys. Res.* **1996**, *101*, 22869.
(9) Fujita, S.; Takahashi, A. *Report T93091*; Central Institute for Electric Power Ind: Tokyo, 1994.
(10) Wolff, G. T. *Atmos. Environ.* **1984**, *5*, 977.
(11) Horai, S.; Minari, I.; Migita, Y. *Ann. Rep. Kagoshima Prefect. Inst.* **1993**, *9*.
(12) Coude-Gaussen, G.; Rogon, P.; Bergametti, G.; Gomes, L.; Strauss, B.; Gros, J. M.; Coustumer, M. N. *J. Geophys. Res.* **1987**, *D8*, 9753.
(13) Tsyganenko, A. A.; Mardilovich, P. P. *J. Chem. Soc., Faraday Trans.* **1996**, *23*, 4843.
(14) Knötzinger, H.; Ratnasamy, P. *Catal. Rev. Sci. Eng.* **1978**, *1*, 31.
(15) Wittbrodt, J. M.; Hase, W. L.; Schlegel, H. B.; *J. Phys. Chem. B* **1998**, *102*, 6539.
(16) Dai, Q.; Robinson, G. N.; Freedman, A. *J. Phys. Chem. B* **1997**, *101*, 4940.
(17) Craciun, R.; Miller, D. J; Dulamita, N.; Jackson, J. E. *Prog. Catal.* **1996**, *5*, 55.
(18) Griffith, P. R.; Fuller, M. P. *Advances in Infrared and Raman Spectroscopy*; Clark, R. J. H., Hester, R. E., Eds.; Heyden and Sons: London, 1983; Vol. 9.
(19) TeVrucht, M. L. E.; Griffith, P. R. *Appl. Spectrosc.* **1989**, *43*, 1492.
(20) Kroetsky, C. M.; Sverjensky, D. A.; Salisbury, J. W.; D'Aria, D. M. *Geochim. Cosmochim. Acta* **1997**, *11*, 2193.
(21) Nakamoto, K. *Infrared and Raman Spectra of Inorganic and Coordination Compounds Part A*, 5th ed.; John Wiley & Sons: New York, 1997.
(22) Vogt, R.; Finlayson-Pitts, B. J. *J. Phys. Chem.* **1994**, *98*, 3747.
(23) Smith, D.; James, D. W.; Devlin, J. P. *J. Chem. Phys.* **1971**, *10*, 4437.
(24) Hadjiivanov, K.; Bushev, V.; Kantcheva, M.; Klissurski, D. *Langmuir* **1994**, *10*, 464.
(25) Peters, S. J.; Ewing, G. E. *J. Phys. Chem.* **1996**, *100*, 14093.
(26) Goodman, A. L.; Miller, T. M.; Grassian, V. H. *J. Vac. Sci. Technol. A* **1998**, *4*, 2585.

(27) Pozdnyakov, D. V.; Filimonov, V. N. *Adv. Mol. Relax. Processes* **1973**, *5*, 55.
(28) Hitchman, M. A.; Rowbottom, G. L. *Coord. Chem. Rev.* **1982**, *42*, 55.
(29) Frunza, L.; Catana, G.; Stoenescu, D. N.; Vilcu, R. *Rom. J. Phys.* **1995**, *6*−*7*, 1.
(30) Herring, A. H.; McCormick, R. L. *J. Phys. Chem. B* **1998**, *102*, 3175.
(31) Miller, T. M.; Grassian, V. H. *Geophys. Res. Lett.* **1998**, *20*, 3835.
(32) Ritzhaupt, G.; Devlin, J. P. *J. Phys. Chem.* **1991**, *95*, 90.
(33) Parkyns, N. D. Adsorption Sites on Oxides. In *Proceedings of the Fifth International Congress on Catalysis*, Miami Beach, FL, August 20−26, 1972; Hightower, J. W., Ed.; 1972; 12−255.
(34) Morterra, C.; Magnacca, G. *Catal. Today* **1996**, *27*, 497.
(35) Dyer, C.; Hendra, J.; Forsling, W.; Ranheimer, M. *Spectrochim. Acta* **1993**, *49A* (*5/6*), 691.
(36) Baumgarten, E.; Wagner, R.; Lentes-Wagner, C. *Fresenius J. Anal. Chem.* **1989**, *335*, 375.
(37) Nelli, C. H.; Rochelle, G. T. *Ind. Eng. Chem. Res.* **1996**, *35*, 999.
(38) Lee, M. R.; Allen, E. R.; Wolan, J. T.; Hoflund, G. B. *Ind. Eng. Chem. Res.* **1998**, *37*, 3375.
(39) Underwood, G. M.; Miller, T. M.; Grassian, V. H. *J. Phys. Chem. A* **1999**, *103*, 6184.
(40) NASA Panel for Data Evaluation: Chemical Kinetics and Photochemical Data for Use in Stratospheric Modelling. *JPL Publ.* **1997**, *12*, 142.
(41) Langer, S.; Pemberton, R. S.; Finlayson-Pitts, B. J.; *J. Phys. Chem. A* **1997**, *101*, 1277.
(42) Vogt, R.; Elliott, C.; Allen, H. C.; Laux, J. M.; Hemminger, J. C.; Finlayson-Pitts, B. J. *Atmos. Environ.* **1996**, *10/11*, 1729.
(43) Judeikis, H. S.; Siegel, S.; Stewart, T. B.; Hedgepeth, H. R.; Wren, A. G. Laboratory Studies of Heterogeneous Reactions of Oxides of Nitrogen. *Nitrogeneous Air Pollutants − Chemical and Biological Implications*, Grosjean, D., Ed; Ann Arbor Science Publishers Inc.: Ann Arbor, MI, 1979; pp 83−109.
(44) Davids, J. A.; Cox, R. A. *J. Phys. Chem. A* **1998**, *102*, 7631.